Green synthesis of Zinc sulphide (ZnS) nanostructures using *S. frutescences* plant extract for photocatalytic degradation of dyes and antibiotics

To cite this article: Shonisani Munyai *et al* 2022 *Mater. Res. Express* **9** 015001

Materials Research Express

PAPER

Green synthesis of Zinc sulphide (ZnS) nanostructures using *S. frutescences* plant extract for photocatalytic degradation of dyes and antibiotics

Shonisani Munyai, Louisa M Mahlaule-Glory and Nomso Charmaine Hintsho-Mbita[1]

Department of Chemistry, DSI/NRF CoE in Strong Materials, University of Limpopo, Sovenga, Polokwane, 0727, South Africa
[1] Postal address: Department of Chemistry, University of Limpopo, Private Bag X 1106, Sovenga 0727, Polokwane, South Africa

E-mail: nomso.hintsho-mbita@ul.ac.za

Keywords: Zinc Sulphide nanoparticles, dyes, pharmaceuticals, green synthesis

Supplementary material for this article is available online

OPEN ACCESS

RECEIVED
9 November 2021

REVISED
13 December 2021

ACCEPTED FOR PUBLICATION
16 December 2021

PUBLISHED
6 January 2022

Abstract

Pollutants such as dyes and pharmaceuticals have become a problem in the environment, thus there is a need to find multifunctional materials that are safe and can be used for the removal of various pollutants. In this study, we report on the synthesis of Zinc sulphide (ZnS) nanostructures and their use as photocatalysts for the degradation of dyes and various antibiotics. Fourier transform infrared spectroscopy (FTIR) confirmed the functional groups found in plants and these were linked to the biomolecules identified through Liquid chromatography-mass spectrometry (LCMS). Ultraviolet-visible spectroscopy (UV–vis) and x-ray diffraction (XRD) confirmed the formation of the ZnS nanostructures. Thermal Gravimetric Analysis (TGA) and Brunner Emmet Teller (BET) confirmed the material was thermally stable up until 480 °C and mesoporous in nature, respectively. Scanning electron microscope (SEM) and transmission electron microscope (TEM) showed that the material is spherical in shape and energy dispersive spectroscopy (EDS) further corroborated their formation. From the degradation analysis, 90% of the malachite green (MG) dye could be degraded in 60 min at optimum conditions (pH 6, 25 mg and 10 mg l^{-1}) and the holes were responsible for the degradation. Lastly, when tested against antibiotics, the ZnS material managed to degrade both the sulfisoxazole (SSX) and sulfamethoxazole (SMX). These results showed that the ZnS nanoparticles could be used as a multifunctional material for the degradation of various pollutants.

1. Introduction

Water scarcity has become a threat to the human kind for some decades. The reports from the World Health Organization estimated that about 1.1 billion of people are unable to access safe and clean water worldwide. This is as a result of industrialization, urbanization, climate change, human activities and agricultural activities [1]. The number of contaminants found in our water streams has increased over the years in particular the dyes and antibiotics [2]. This is due to the over reliance on organic dyes by the textile industry especially for dying cloths, thus causing leaching. Also with the high number of patients being prescribed antibiotics such as sulfisoxazole (SSX) and sulfamethoxazole (SMX) due to various ailments, these drugs tend to be excreted through urine and faeces, causing a high concentration in our water streams [3, 4]. These pollutants if they are not attended to and exceed the permissible levels, they can be detrimental to both human and aquatic life. Hence, the use of semiconductor photocatalyst has emerged as a promising way to remove these pollutants from wastewater. Several methods have been used for the removal of organic pollutants such as dyes, but because these dyes consist of the complex structure, most methods such as reverse osmosis, adsorption, electrocoagulation etc have fallen short [5]. These methods either rely on expensive adsorbents, produce secondary pollutants, need multiple steps or require high energy, which may not be feasible when one considers cost factors. Antibiotics are

also a concern because they are among the fastest-growing new toxins in our waterways, it is imperative to find methods and materials that are environmentally friendly and can be used to target various pollutants [3].

The photocatalysis method has been extensively used in the last few decades due to its fast oxidation, non-toxicity and ability to degrade pollutants into environmentally viable materials [6]. This method uses light to generate electrons and holes which promote the generation of reactive species that are effective oxidizers [7, 8]. The pace in which the oxidation and reduction process is occurring during photocatalytic activity determines its removal efficiency.

Semiconductor Zinc sulphide (ZnS) nanostructures is one of the well-studied material which have been employed as a photocatalyst for removal of organic pollutants like Methyl orange (MO), Methylene blue (MB) and Rhodamine blue (RhB). ZnS is known to have a wide band gap, superior light absorption and photocatalytic properties [4]. Moreover, they also have interesting optical and electronic properties. The semiconductor belongs to the II-VI group and has the band gap ranging from 3.63 to 3.92 eV [2]. It normally crystallizes to hexagonal wurzite and cubic zinc blende structure. The ZnS nanostructures have been synthesized using different conventional methods. Salavati-Niasari *et al* [5] prepared wurtzite ZnS nanorods via the hydrothermal route, with the diameter ranging from 40 to 200 nm. La Porta *et al* [6] also synthesized cubic ZnS nanoparticles using microwave synthesis. In other studies, Huo *et al* [7] employed a solid-state method for the synthesis of their particles. Though these conventional methods used had successfully synthesized these particles, they do suffer from some limitations. Generally, it is known that nanostructures agglomerate fast in the presence of capping agents [8, 9]. Furthermore, these methods use toxic chemicals which result in poor control of particle size, shape and reproducibility [4]. For those particular reasons, suitable green synthesis methods have been developed in order to avoid such limitations. The green synthesis methods include the uses of plants, bacteria, fungi and algae for the synthesis of nanostructures. Among all these plants are preferred because of their ease at handling and accessibility [10]. *Sutherlandia frutescens* is the plant of interest which has been traditionally used as a tonic. It has also been reported that its consists of phytochemical like GABA, canavanine and flavonols. The plant has been used before for the synthesis of ZnO [8] and CdS [11] nanoparticles, so this is evident enough that the plant can be used as a reducing and stabilizing agent for the nanostructures. The green synthesis of sphere-like ZnS nanoparticles with an average size of 45 nm have been reported using *Corymbia citriodora* leaf extract [12]. These nanoparticles were evaluated for the photodegradation of MB dye and they showed excellent performance whereby 96% of the dye was degraded using UV light. Senapati *et al* [13] used *Elaeocarpus floribundus* leaf extract to synthesize spherical ZnS nanoparticles with a small particle size of 3–8 nm, which were investigated for their electrical properties.

In light of these, there are not many studies where green derived materials have been used for the degradation of antibiotics. In this study, the ZnS nanostructures were synthesized using *Sutherlandia frutescence* (*S. frutescence*) plant extracts. The degradation of MG dye at various conditions is investigated. And lastly, we report on the degradation of antibiotics, SMX and SSX using green ZnS for the first time.

2. Materials and methods

2.1. Materials and reagents

Sutherlandia frutescens (*S. frutescence)* tea was purchased from a local store in Polokwane, RSA. MG, SMX, $ZnCl_2$ and Na_2S were all purchased from Protea Labs, South Africa. SSX was given by Dr T Leboho from the Chemistry Department, University of Limpopo, RSA.

2.2. Extraction of *S. Frutescence* plant and synthesis of ZnS nanoparticles.

S.frutescence extract was prepared using the tea infusion method as described by Mahlaule-Glory without any modification [8]. The extract was kept in the refrigerator at 4 °C and used for further reaction analysis. For the synthesis of ZnS nanoparticles, in 100 ml of *S. frutescens* plant extract, an amount 2.5 g of $ZnCl_2$ and Na_2S salt were added while stirring, and the solution was heated at 80 °C for 1 h. Thereafter, the solution was centrifuged at 2000 rpm for 15 min, washed three times with distilled water and dried in the oven at 80 °C. The final powder was crushed and calcined at 500 °C for 2 h.

2.3. Characterization

The phytochemicals present in *S. frutescens* extracts were confirmed by a synats G_2 quadrupole time-of-flight (QTOF) mass spectrometer (MS) connected to a water acquity ultra-performance liquid chromatography analysis. The functional groups of the materials were analyzed using FTIR, Perkin Elmer spectrum 100 FT-IR spectrometer in a scan range of 500–4000 cm^{-1}. The multi-purpose x-ray diffractometer (XRD) D8-Advance from Bruker in a scan range of 15–75 2θ was used to determine the crystallite size, crystallinity and phase identification of the synthesized materials. UV–vis, Beckman Coulter DU 730 UV–vis spectrophotometer was

used for optical analysis and to track the degradation of the dye and antibiotic, with wavelengths of 665 and 285 nm, respectively. TGA Q500 V20.13 Build 39 was used for the determination of the thermal stability and weight loss of the material using a Perkin Elmer Pyris instrument. For each run, roughly 10 mg of the sample was used and the temperature of focus was between 35 and 900 °C and the reaction taking place at a rate of 10 °C min^{-1}. Tristar II BET equipment manufactured by Micromeritics (USA) was used to determine the surface area of the nanostructures. Energy Dispersive x-ray Diffraction Spectroscopy (EDS) was used to analyse elemental composition and mapping, Transmission Electron Microscopy (TEM), JEOL JEM-2100 electron microscope (Japan) operated at an accelerating voltage of 200 kV and Scanning Electron Microscopy (SEM), Hitachi X 650 Scanning electron microscope was used for morphology.

2.4. Photocatalytic

The effect of the nanophotocatalysts was demonstrated by photodegradation of MG under the 300 W lamp light source. Following and modifying the methods reported by Ngoepe *et al* [14], the effect of pH (4–10), catalysts dosage (25–100 mg) and dye concentration (5–20 mg l^{-1}) was investigated. Prior to UV irradiation, the solution containing the nanophotocatalysts was stirred continuously for about 30 min in the dark to reach an adsorption-desorption equilibrium so that the degradation efficiency can be influenced by photodegradation. After reaching the equilibrium, the system was subjected to UV irradiation using a 300 W light source. The distance between the light source and solution surface was kept constant at about 5 cm throughout the photocatalytic experiments. Briefly, 5–20 mg ml^{-1} concentration of MG dye pollutant was prepared and 25–100 mg of the dosage was added in a 250 ml solution in a 500 ml beaker. The samples were irradiated for 60 min and analysis for the degree of degradation was taken at 15 min intervals. To calculate the % degradation for each experiment, the formula denoted as equation (1) was used.

$$(\%)D = \frac{A_0 - A_t}{A_0} \times 100 \tag{1}$$

Where A_0 is the initial absorbance and A_t is the final absorbance. The kinetics of photocatalytic reaction of MG was calculated using this formula:

$$\ln\left(\frac{A_o}{A_t}\right) = kt \tag{2}$$

Where A_0 is the initial absorbance, A_t is the final absorbance, k being the degradation kinetic of the photocatalyst and t is the irradiation time.

Similarly, the pharmaceutical pollutants, SSX and SMX were degraded following the same method as above. However, the operating parameters were different and were recorded as follows: natural pH, 25 mg dosage, 10 mg ml^{-1} concentration, time duration of 60 min and the wavelength of the light used was 300 nm. The decaying and the degradation of the pollutant was recorded at 285 nm.

2.5. Reusability and trapping studies

Reusability studies were conducted for 4 cycles under the same conditions as the actual degradation run. For each run, the sample was filtered after the degradation, washed and dried and reused. Also, the trapping of active species experiments was conducted using propan-2-ol (1 M), silver nitrate (0.1 M), EDTA (0.1 M) and p-Benzoquinone (0.1 M) to evaluate the effect of hydroxide ($OH^{\cdot}$) radicals, electrons ($e^{\cdot}$), holes (h^{+}) and superoxide ($O_2^{\cdot}$) respectively. The concentration used for the scavenger was chosen based on what has been reported on literature. For these experiments, the blank did not contain any of these trappers, then for the trapping studies, scavengers as noted were added.

3. Results and discussion

3.1. Qualitative analysis of *S. frutescens* plant extract

LC-MS was used to investigate the qualitative analysis of *S. frutescens* plant extract. The possible compounds obtained are presented in table 1 and they were determined through the mass to charge chromatogram.

Table 1 sums up the LC-MS data of the phytochemicals present in the *S. fructescens* plant extract. The mass to charge values 149.04, 191.02, 178.05, 161.04 and 723.18 were corresponding to the biomolecules xylopyranoside, 2,3-diketogulonate, 1,4-Glucarolactone, N-Acetylanthranilate, 4,5-dihydroxyoxane-2-carboxylate and Pelargonidin 3-(6′-malonylglucoside)—5-(6′-acetylglucoside) respectively and they are shown in figure 1. The recorded compounds have been investigated previously for different biological activities including cytotoxicity and antioxidant studies. From the results obtained, the *S. fructescens* plant extract contains a higher content of phenolic, glycosides and flavonoids group. In the study done by Mahlaule-Glory *et al* [8] and

Table 1. Different compounds identified using LC-MS for *S. frutescens* extract.

Molecular formula	Molecular weight	Compound name	Group name	Biological activity
$C_5H_9O_5$	149.04	xylopyranoside	Glycosides	Cytotoxicity assessment [15]
$C_6H_7O_7$	191.02	2,3-diketogulonate	Phenolic	Antioxidant activity [16]
$C_9H_8NO_3$	178.05	N-Acetylanthranilate	Alkaloids	Urinary-metabolite profiles [17]
$C_6H_9O_5$	161.04	4,5-dihydroxyoxane-2-carboxylate	Phenolic	Not reported
$C_{32}H_{35}O_{19}$	723.18	Pelargonidin 3-(6′-malonylglucoside)−5-(6′-acetylglucoside)	Flavonoids	Not reported

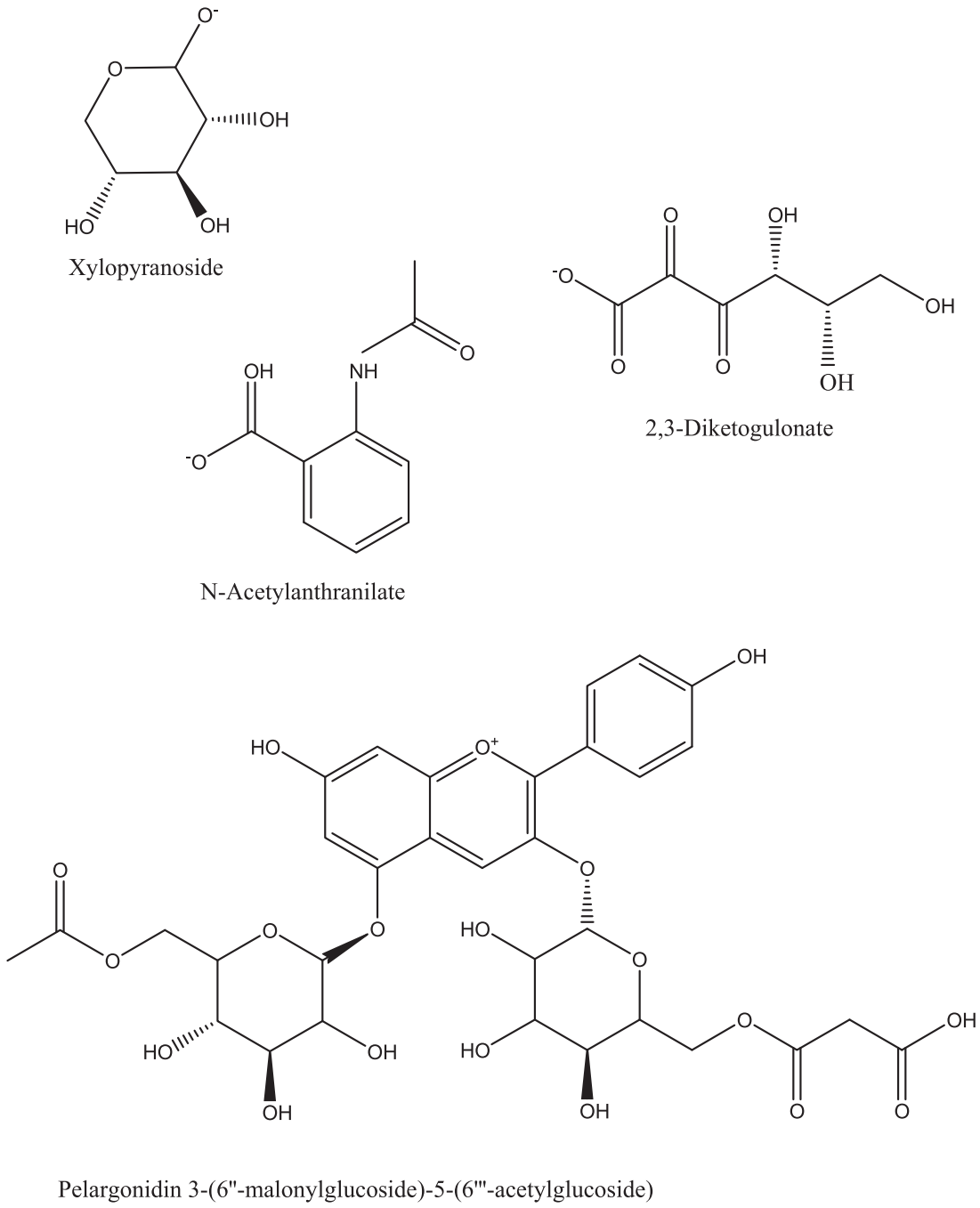

Figure 1. Chemical compound found in *S. fructescens* plant extract.

Lei *et al* [9], the glycosides and flavanols compounds were identified to be in highest content. FTIR was done to further confirm the functional groups presence in the plant.

3.2. Spectroscopic analysis using FTIR

FTIR analysis was used to determine the functional groups involved in the synthesis of ZnS nanostructures using *S. fructescens*. and the ones present in the *S.frutescens* plant extract.

Figure 2 shows the FTIR spectra of the *S. fructescens* plant and the SF-ZnS. The *S. fructescens* plant extract spectra exhibited vibrational stretching at 3400 cm^{-1}, 2222 cm^{-1}, 1017 cm^{-1} and 1645 cm^{-1}. The strong broad absorbance peak at 3400 cm^{-1} is due to hydroxyl group (O–H) shifting, the small and sharp peaks at 1339 cm^{-1} and 1017 cm^{-1} are as a result of C–N and C–O stretching which might be due to amino groups [13]. The carboxylic group is responsible for the absorbance peak at 1645 cm^{-1} which matches the C=O groups. These peaks were also observed and deposited on SF-ZnS. The Zn-S vibrational stretching was observed around 680 cm^{-1} in the fingerprint region confirming the formation of ZnS nanostructures synthesized using *S. fructescens* plant. Since several phytochemicals have been identified from the plant extract, and these are used as reducing

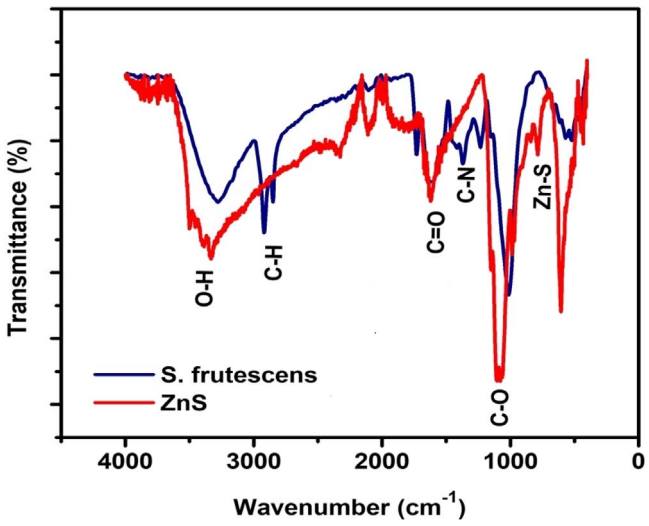

Figure 2. FTIR spectra of *Sutherlandia fructescens* plant with SF-ZnS nanostructures.

agents, the mechanism of formation can be proposed. The proposed mechanism for the formation of ZnS nanostructures using *S. fructescens* plant extract is as follows. Firstly, the phytochemicals such as flavonoids, alkaloids, glycosides and phenolic of *S. fructescens* plant extract bind and reduce the $ZnCl_2$ into Zn^{2+} ions. Thereafter, the added $Na_2S.9H_2O$ forms the S^{2-} ions which bind to the zinc metal connected to the phytochemicals. Then nucleation and growth process occurs on the nanostructures thus the formation of ZnS nanostructures. The phytochemicals on the *S. fructescens* plant extract bound to the surface of the ZnS nanostructures prevented the agglomeration of the particles while stabilizing the nanostructures. Further, because the phytochemicals comprise of carbonyl groups that have the capacity to direct the shape, the capping of the ZnS nanostructures also occurs. From the FTIR spectrum, the results reveal that the flavonol, canavanine and Gaba with the functional groups like hydroxyl, amino and carboxylic acids might have been absorbed on the surface of the ZnS nanostructures and this suggests that they played an important role during their formation. To further confirm the formation of this material, XRD analysis was conducted.

3.3. Crystallinity and peak identification studies

The phase structure of the synthesized SF-ZnS nanostructures was evaluated using XRD as presented in figure 3. The diffraction peaks on SF-ZnS nanostructures shows it consists of hexagonal phases which are indexed from JCP2–80–0007. The reflective peaks at 27.2°, 28.8°, 30.9°, 40.1°, 48.1°, 52.4°, 56.2°, 57.1°, 58.3°, 59.7°, 64.24° and 73.9° correspond to (100), (002), (101), (102), (110), (103), (200), (112), (201), (202) and (203) planes. The mean crystalline size of SF-ZnS nanostructures was determined by the Scherer expression;

$$D = \frac{k\lambda}{\beta \ \mathrm{Cos}\ \theta} \tag{3}$$

Where K = 0.9, indicates the constant shape factor, λ represents the x-ray wavelength of CuK_α (1.5404 Å), β is the peak full width at half maximum (FWHM) of the diffraction peak, θ is the bragg's diffraction angle and D is the average crystallite size of the nanostructures.

The average size of the SF-ZnS nanostructures synthesized was estimated to be around 41.22 nm. The calculation of the size was done based on the intense peak using the FWHM of the XRD peak broadening. Additionally, the lattice spacing was estimated using Bragg's formula;

$$d = \frac{\lambda}{2 \sin \theta} \tag{4}$$

where d is the lattice spacing, θ is the Bragg's angle, and λ is the wavelength of x-ray. Table 2 shows the diffraction data that justifies the formation of wurtzite hexagonal structure of SF-ZnS nanostructures with the lattice parameter of a = 3.777 Å and c = 6.188 Å. Similarly, in the study conducted by Sathishkumar *et al* [18] using the ZnS nanoparticles synthesissed by *tridaxprocumbens* plant extracts, they showed that the material had a hexagonal wurtzite structure. Further, their calculated crystalline grain size was found to be 40 nm. ZnS nanoparticles with hexagonal wurzite phase was also synthesized using plant extracts of *Tridax procumbens* by Kannan *et al* [19]. The crystalline pattern also showed that there were a few impurity peaks, and these impurities are suspected to be from plant phytochemicals, they were also ideintified in EDS analysis. Their calculated crystalline size by Debye–Scherrer equation was found to be 22.70 nm. Further, the crystalline growth of ZnS

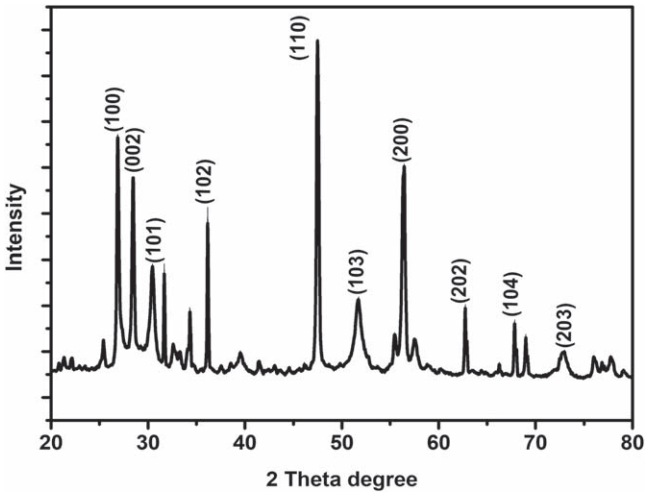

Figure 3. X-ray diffraction pattern of the synthesized SF-ZnS nanostructures.

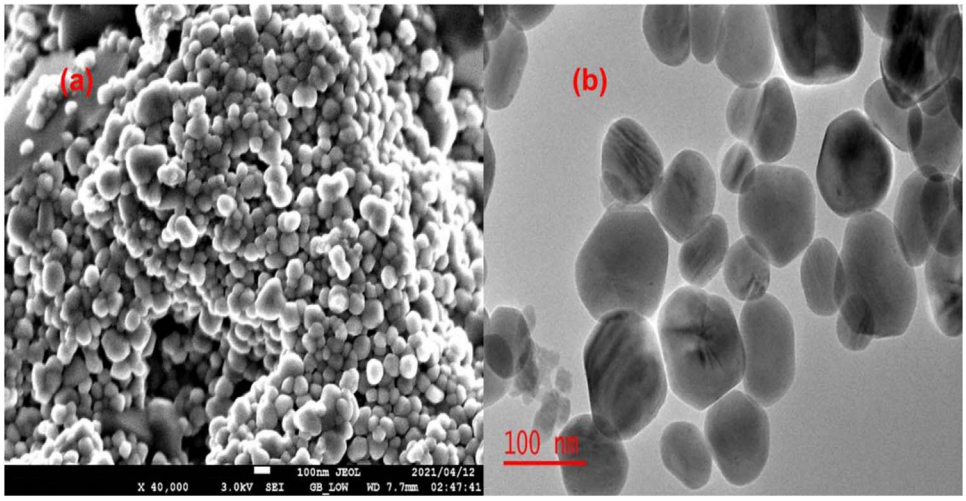

Figure 4. (a) SEM image and (b) TEM image of SF-ZnS nanostructures.

Table 2. Summary of the diffraction data of the SF-ZnS nanostructures synthesised using *S. fructescens* plant extract.

Bragg angle 2θ (degree)	FWHM	Lattice planes ($h\,k\,l$)	Inter-planar spacing d (nm)	Crystallite sizeD (nm)
47.5020	0.2852	(110)	3.8251	41.2295

was reported to be due to the biomolecules like phenols, alkaloids, flavonoids and saponins. To obtain more information on the structure of the material, morphological analysis was also conducted.

3.4. Morphological and elemental analysis

The SF-ZnS nanostructures were characterized using HRSEM and TEM. From figure 4(a), SEM shows that the morphology of the particles were spherical in shape and appear as clusters. Using image J, the particle sizes were measured to be between 70–170 nm as shown on the histogram (figure 4(b)). TEM analysis also confirmed the formation of large particles of spherical morphologies with some clustering. Bai *et al,* synthesized ZnS nanoparticles using *Rhodobacter sphaeroides* [4]. Upon conducting a synthesis time study, increasing the time interval also led to an increased average diameter of 4, 8, 30 and 105 nm respectively. The increment in the average diameter was stated to be due to the nucleation effect which leads to the agglomeration of small particles thus larger particles are also identified in our TEM results (figure 4(b)). A controlled particle size is one of the most important standards in the area of green derived nanomaterials since it has an influence on the application

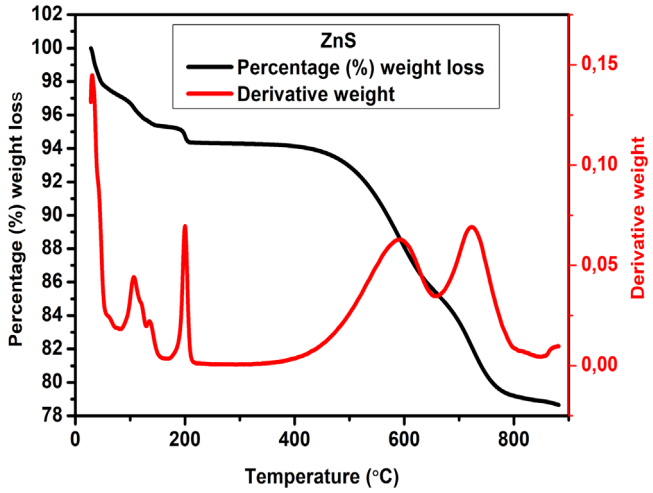

Figure 5. (a) TGA (percentage (%) weight loss and (b) derivative curve for the SF-ZnS nanostructures.

of the nanostructures. As observed in the TEM image, the particle size of SF-ZnS nanostructures is uniform and large as a results of plant extract covering the surface of SF-ZnS. When the concentration of phytochemicals which are responsible of mediating the synthesis of SF-ZnS is low the interaction is minimum leading to an increase of particle size.

Energy dispersive x-ray spectroscopy (EDS) also provided information about the elemental composition and purity of SF-ZnS nanostructures. Their elemental analysis was obtained from the selected regions of the SEM image. The spectra indicated the presence of zinc and sulphur which confirms indeed that the synthesised ZnS using plant extract of *S. fructescens* were formed. The presence of other elemental peaks like C, O, Al, Si, Cl, K and Ca maybe due to surface contamination and absorbed residual surfactants on the nanostructure [20]. Moreover, they might be as a result of unreacted biomolecules from the *S. fructescens* plant extract. Hussain and co-workers [21] reported that the impurities on the ZnS nanoparticles demonstrated on their EDX spectra were coming from the proteins or enzymes of the *A. bisporus* extract. Thermal stability test using TGA weight loss were conducted to determine the material's stability.

3.5. Thermal stability studies

Thermogravimetric analysis is important in determining the thermal stability of the materials. The TGA and DTA curve of SF-ZnS nanostructures are shown in figures 5(a) and (b). From the TGA curve in figure 5(a), the decomposition of the nanostructures started from 100 °C up until 800 °C. Initially, the percentage (%) weight loss (1.46%) recorded corresponded to the exothermic peak at 106 °C on the DTA curve which was attributed to the loss of moisture from the sample. The peaks at 200 °C and 590 °C with the percentage weight loss of 1.20% and 7.60% respectively were attributed to the breakdown and oxidation of phytochemicals on the plants (biomolecule on *S.frutescens* plants). Lastly, a large exothermic peak at 723 °C which might be because of the crystallization of SF-ZnS nanostructures or the loss of the remaining residues on the sample and 1.61% of the weight loss was observed. Similarly, the same results were recorded by Senapati *et al* [22] for the synthesis of ZnS nanoparticles using starch. The BET results were explored in order to have a better understanding of the surface area, pore size and volume of the SF-ZnS nanostructures.

3.6. Surface area measurements of SF-ZnS nanostructures

Figures 6(a)–(c) illustrate the Nitrogen adsorption-desorption isotherms together with the pore diameter and surface area plot of the SF-ZnS nanostructures. From figure 6(a) clearly shows that the isotherms belongs to the standard of IUPAC recommendation type IV isotherms which exhibit a monolayers then followed by multilayer adsorption on the ZnS nanostructures. The surface area of the synthesized SF-ZnS nanostructures is 6.6973 m^2 g^{-1}. The Barrett–Joyner–Halenda (BJH) technique was used to calculate the pore volume and pore diameter. The pore volume and pore diameter of the SF-ZnS nanostructures were found to be 0.018494 cm^3 g^{-1} and 36.88 nm respectively. The plot of pore diameter relative to pore volume confirm the presence of mesoporous structure for SF-ZnS (average pore size between 2–50 nm).

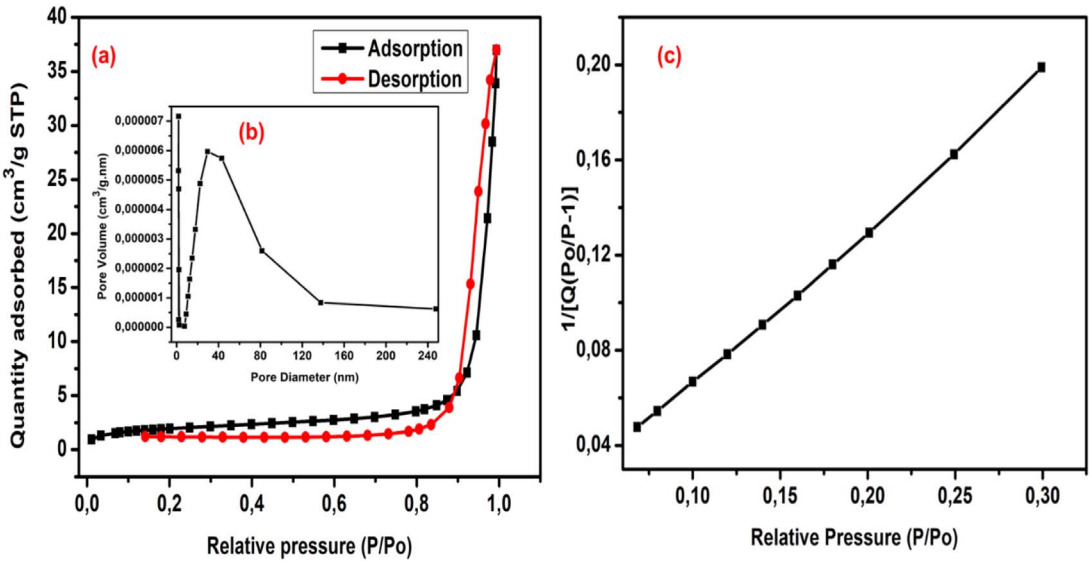

Figure 6. (a) Nitrogen adsorption - desorption isotherm (b) pore diameter and (c) surface area plot for SF-ZnS nanostructures.

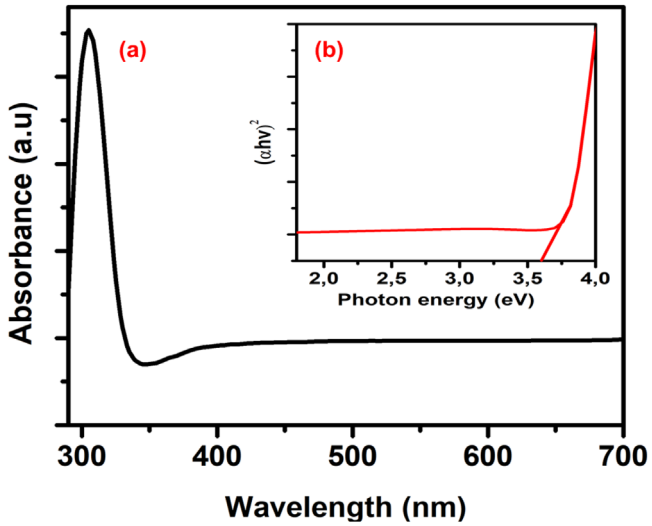

Figure 7. (a) Optical absorbance and (b) tauc's plot of SF-ZnS nanostructures.

3.7. Optical properties of SF-ZnS nanostructures

The absorption spectra of SF-ZnS nanostructures was analysed in the range between 300 to 700 nm. The optical absorption spectrum of SF-ZnS nanostructures displayed the absorption peak at 304 nm as seen in figure 7(a). This suggests that the absorption band was blue shifted due to the formation of SF-ZnS nanostructures. In a study done by Senapati *et al* [23], the ZnS nanoparticles synthesized using mushroom *Pleurotuss ostreatu* reported that their absorption peaks were blue shifted because of the electrons stimulation from the valence band to the conduction band. Further, this was also observed in the study where they used glucose carboxymethylcellulose (CMC) for the synthesis of ZnS nanoparticles. They demonstrated that their absorption band edge was observed between 270 and 330 nm, and this was blue shifted [24]. The same trend was also observed in studies investigated by Huo *et al* , Samanta *et al* and Lalithadevi *et al* [25–27]. The band gap energy for the nanostructures was estimated using Tauc plot. The calculations were done using the expression $\alpha hv = (hv\text{-}Eg)^n$: where, h is for the Planck's constant, α stands for the absorption coefficient, $h\nu$ is for the photon energy and E_g is for the optical band gap. The Tauc plot of $(\alpha hv)^2$ against photon energy (eV) is shown with the respective UV–vis spectrum for nanostructures. The tangent line depicts the band energy on taucs plot. The direct band gap energy was obtained to be 3.60 eV for SF-ZnS. The obtained band gap energy of the semiconductor SF-ZnS nanostructure was lower than the ZnS bulk. This case was also observed in the study

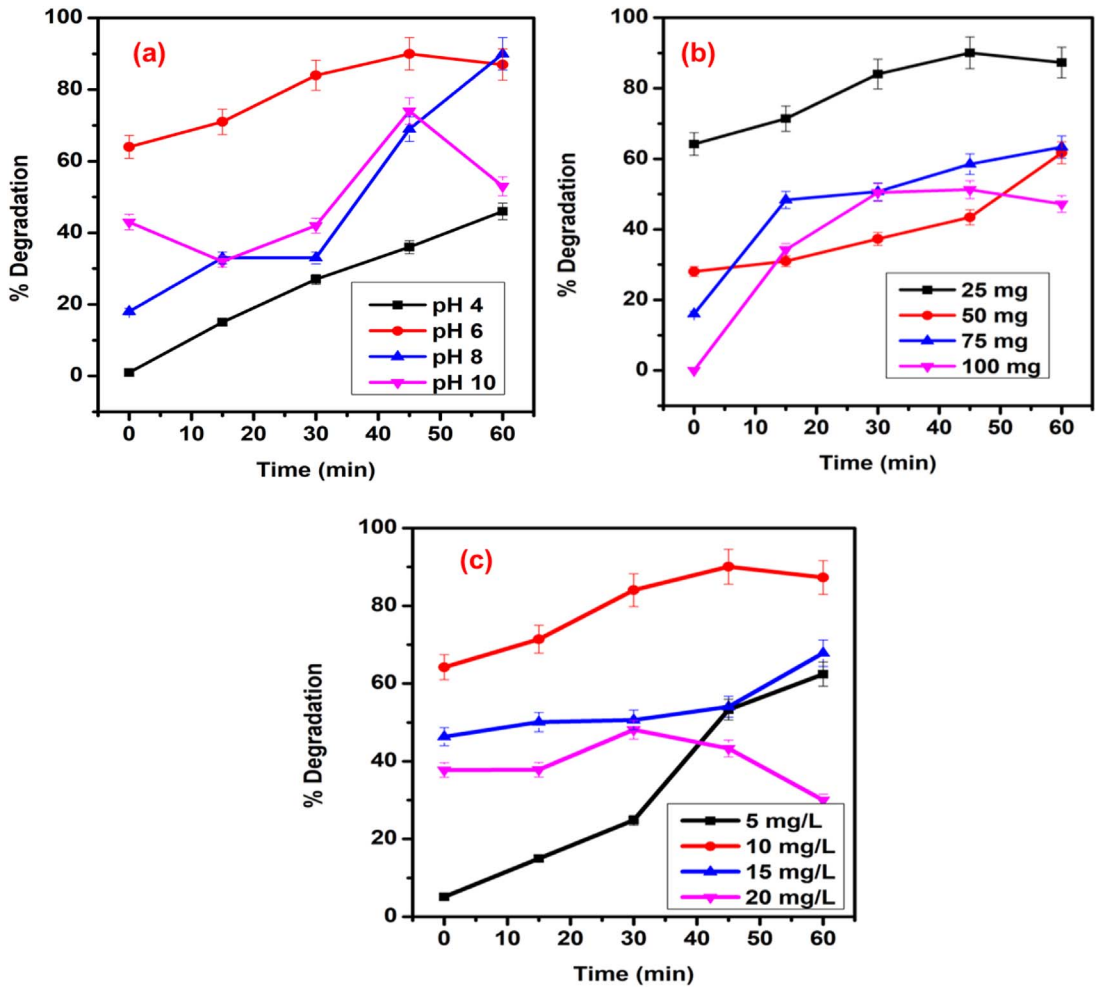

Figure 8. (a)–(c). MG photocatalytic activity as a function of (a) pH, (b) dose, and (c) concentration.

where Kannan *et al* [28], used *Acalypha indica* and *Tridax procumbens* plant extract for the synthesis ZnS nanoparticles. This was because of an increasing particle size which occurred during the growth period of grains thus resulting in the decrease in defect of band edge of wavelength in the UV region.

3.8. Photocatalytic activity of SF-ZnS nanostructures synthesised using *S. fructescens* plant

The photocatalytic activity of SF-ZnS was also investigated against malachite green (MG) dye and antibiotics, sulfisoxazole (SSX) and sulfamethoxazole (SMX). The effect of pH, catalyst loading and dye concentration were investigated for the degradation of MG.

3.9. Studies of the different pH, dosage and concentration values for the photocatalytic activity of malachite green using SF-ZnS nanostructures

The photocatalytic activity of SF-ZnS nanostructures was investigated against the malachite green dye at the interval of 15 min within 60 min and it was analysed from pH 4–10 (figure 8(a)). The semiconductor ZnS is an amphoteric material, which means that there is change in the surface charge of ZnS with the changes in pH values, thus it is important to conduct the effect of pH [29]. The degradation efficiency of MG was found to be 46, 90, 90 and 74% for pH 4, 6, 8 and 10 respectively. From this analysis, it can be noted that pH 6–8 produced the highest degradation of 90%. Generally, since MG is a cationic dye it favours alkaline medium for its removal. When the pH of the medium was increased there was a promotion of reactive species (OH radicals) which are essential during degradation. Nevertheless, the degradation efficiency of the SF-ZnS nanostructures reached a plateau at pH 6–8 and started to decrease after pH 8. This could be due the fact that maybe the produced hydroxyl ions were competing with the dye molecules during the process of absorption on the surface catalyst. In addition, at lower pH, it is difficult to form the needed hydroxyl groups to form hydroxyl radicals since it is in acidic medium and as such the removal is reduced. The SF-ZnS nanostructures were further investigated for their kinetics as indicated in table 3 for better understanding towards the photodegradation. The rate constants

Table 3. Kinetics studies of different pH values.

pH	R^2	Rate constant K (min^{-1})
4	0.9645	0.0087
6	0.2199	0.0096
8	0.5869	0.0075
10	0.5666	0.0164

Table 4. The kinetic studies of various dosage photocatalyst.

Dosage	R^2	Rate constant K (min^{-1})
25	0.7806	0.0207
50	0.7796	0.0097
75	0.8339	0.0125
100	0.5820	0.0164

Table 5. Kinetics studies for various concentrations.

Concentration	R^2	Rate constant K (min^{-1})
5	0.9095	0.0165
10	0.7623	0.0209
15	0.6887	0.0076
20	0.1677	0.0021

were found to be 0.00869, 0.0096, 0.00747 and 0.0164 min^{-1} corresponding to pH 4, 6, 8 and 10 respectively. The rate constants revealed that the degradation rate of the dye at pH 6 was multiplied more as compared to other pH values thus there was high efficiency of photodegradation of MG. The kinetic studies conducted on different pH values shows that only one R^2 value was greater than 0.90 which is for pH 4. From these, the kinetics studies for pH 4 were fitted for the pseudo-second order. Though that is the case, still none of them really fitted for the second order kinetics reaction. From the investigation, pH 6 was taken as the optimum value for all the experiments, since it had the highest degradation at the lowest pH and a better degradation rate, compared to the other pHs

The study on the effect of catalyst loading was conducted using several loadings from 25, 50, 75 and 100 mg as displayed in figure 6(b). The degradation efficiency decreased as the catalyst loading increased. The results show that a highest degradation percentage was obtained when 25 mg loading was used. The degradation removal was found to be 90, 62, 63 and 51% corresponding to 25, 50, 75 and 100 mg respectively. When an amount of the dosage catalyst is increased, the degradation efficiency is supposed to increase because of more available active sites. However, this study showed that a further increase in loading resulted in a decrease in the removal efficiency. This may be due to the aggregation of the SF-ZnS photocatalyst which led to the decrease in the surface area of the particles [14]. The photocatalytic activity rate constant values corresponding to the dosage loading 25, 50, 75 and 100 mg were 0.02073, 0.00967, 0.01253 and 0.0164 min^{-1} respectively as summarized in table 4. These rate coefficients follow the order 0.00967, 0.01253, 0.0164 and 0.02073 min^{-1}. The R^2 obtained from the plotted graphs did not fit the second order reaction because their values were too far from the preferred 0.99 value.

After the pH and dosage investigation of SF-ZnS nanostructures, the photocatalytic activity of the photocatalysts in degrading MG with various concentrations (5 $mg\,l^{-1}$ ^{20} $mg\,l^{-1}$) was also evaluated. figure 8(c) shows the degradation plot related to the photocatalytic activity of MG on the effect of concentration. The removal capacity of MG dye decreased as the dye concentration increased. This occurs because as the concentration is increasing, the lights ability to be transmitted into the solution is limited. The increase in light absorption of the dye molecules causes a lesser amount of the photons to hit the surface of the photocatalyst [30]. From the results, the removal efficiency of MG dye using SF-ZnS nanostructures were 62%, 90%, 70% and 30% respectively. The kinetic studies done on different initial concentrations are given on table 5. These values shows that at 10 $mg\,l^{-1}$ concentration of the dye, the k value was greater than when the concentration of the dye was 5 $mg\,l^{-1}$, 15 $mg\,l^{-1}$ and 20 $mg\,l^{-1}$. This indicates that at 10 $mg\,l^{-1}$ the degradation rate of malachite green was faster resulting in a higher photocatalytic activity.

Table 6. Comparative photodegradation studies of green derived ZnS.

Plant or microorganism species	Light	Concentration of dye	Catalyst dosage	Time (min)	Percentage removal (%)	Reference
Tridax procumbens, Phyllanthusnir-uri, and Syzygium aromaticum 90, 92, 95 and 99 for MO	UV	1×10^{-5} M	1.0 mg	180	55, 68, 73 and 81 for MB	[31]
Citrus limetta	sunlight	5 μM	5 mg	150	83	[32]
Acalypha indica and Tridax procumbens	UV	1×10^{-5} M				
	1.0 mg	180	95 and 98	[28]		
Corymbia citriodora	UV	20 mg l^{-1}	20 mg	240	96	[12]
Tridax procumbens	UV	2 mg l^{-1}	10 mg	180	99	[33]
S. frutescens	UV	10 mg l^{-1}	25 mg	60	90	Present study

3.10. Comparison study between green synthesis ZnS materials and their degradation efficiency

For comparison, some previously reported studies are presented in table 6 that demonstrate the photocatalytic activity of green synthesised ZnS nanoparticles. Most of the studies mentioned focused on the photodegradation of dyes like methylene blue, methyl orange and rhodamine B and in almost all of them UV light was used as the light source during the process. Further, these studies were compared with the recent study in terms of light source, dosage, degradation efficiency and the time. In this study MG was used as a model pollutant. From the results as shown in table 6, the ZnS nanostructure synthesised using different plant extracts had a higher percentage degradation (ranging from 55%–99%) over a longer period of reaction time (150–240 min) as compared with the present study of the SF-ZnS. This might be due to different factors such as the morphology, particle size, band gap energy, surface area and the active sites. All these studies achieved the highest degradation efficiency with the minimal dosage photocatalyst. The results in the present study showed that about 90% of the MG dye was degraded in 60 min The plant extract played an important role on their photodegradation efficiency. Through photocatalytic activity, the phytochemicals on the surface of the SF-ZnS nanostructures as seen in FTIR spectrum provide the surface charge to avoid aggregation of the particles hence the nanostructures are stabilized. In addition, these phytochemicals also act as a connection points for establishing phytochemicals-MG molecules complex which promotes the decomposition of MG dye.

3.11. Reusability studies

The reusability and stability studies (figure S4 (available online at stacks.iop.org/MRX/9/015001/mmedia)) of SF-ZnS nanostructures were investigated for four cycles using the optimum conditions of 25 mg of the photocatalyst and 10 mg l^{-1} of the concentration. The results as seen in figure 8 show that the photodegradation of MG using SF-ZnS nanostructures decreased drastically after each cycle, for the successive cycles. Their percentage removal was found to be 90%, 70%, 60% and 57% respectively. This means that as the photocatalyst was used continuously, it was losing its stability hence the excessive decrease in its photocatalytic efficiency. Since the photocatalyst was in small amounts, the filtration and drying process might have contributed to this too much loss of the photocatalyst before the.

It is known that the crucial step in photocatalytic activity is an absorption of dye molecules on the surface of the nanostructures. In the study done by Rajabi *et al* [34], it was reported that the decrease in the photocatalytic efficiency during the reusability studies was because the available active sites were occupied by the absorbed molecules thus this resulted to decrease in photocatalytic activity of the photocatalysts at following cycles. Similarly, this was the same case on the study done by Wang *et al* [35].

3.12. Quenching of active species during photocatalytic activity

Further investigations were carried out to explore the role of different scavengers. For these quenching studies, scavengers such as isopropanol, silver nitrate, EDTA and p-Benzoquinone for hydroxyl radicals, electrons, holes and superoxide respectively were employed. From the bar graph represented in figure 9(f), the addition of those scavengers exhibited that their effect was able to be suppressed. A decrease in the removal efficiency was noticed following the order as $O_2^{\cdot}$, h^+, $OH^{\cdot}$ and $e^{\cdot}$ and 40%, 41%, 48% and 82% was degraded. From the results, the superoxide and holes played a crucial role in the photodegradation of MG, then followed by the OH^- species. In the study done by Samantha *et al* [26], the degradation of RhB dye was suppressed by the presence of silver nitrate as compared to the addition of EDTA and TBA. This meant that e^- was the major oxidative species responsible for degradation of the dye. To further test this material against other pollutants, their efficiency against antibiotics such as sulfisoxazole (SSX) and sulfamethoxazole (SMX).

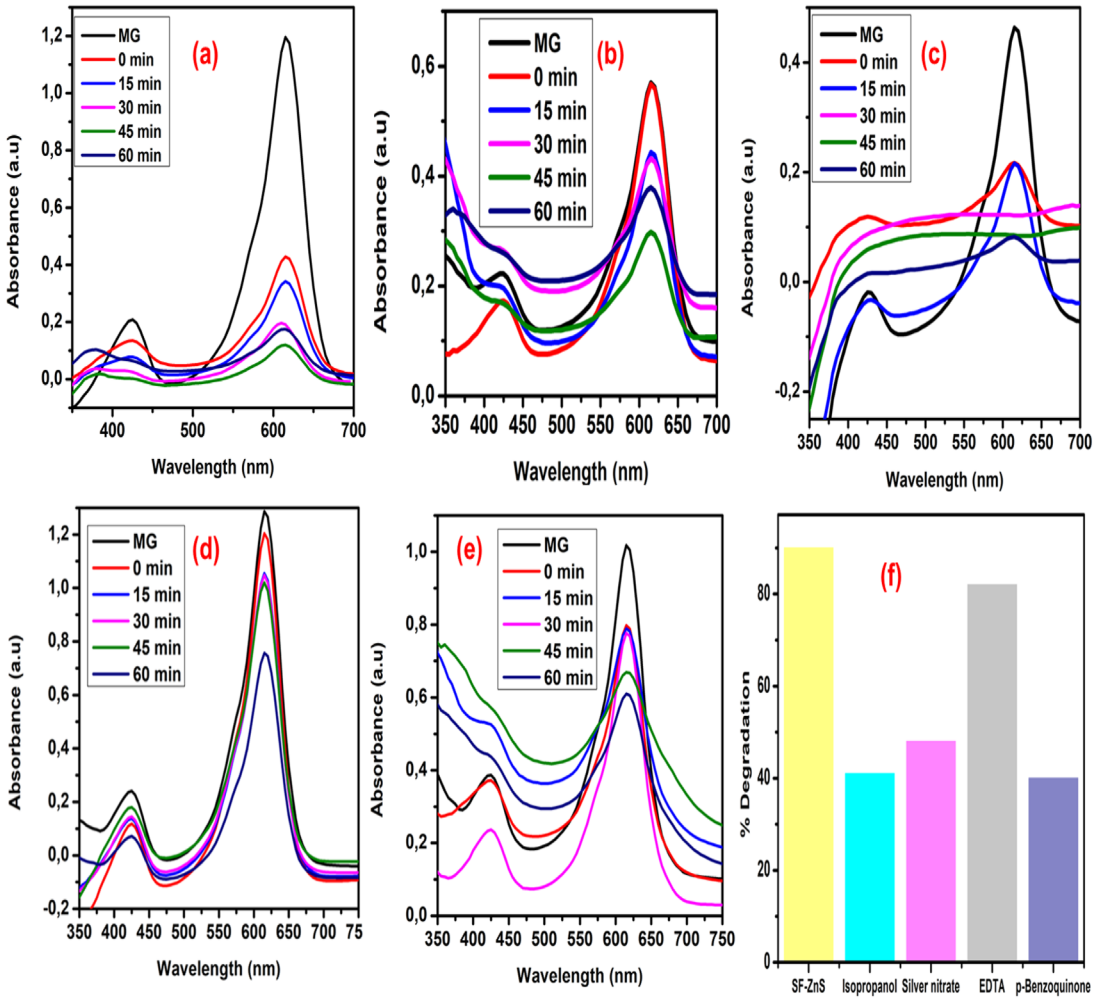

Figure 9. The UV–vis absorption spectrum of photocatalytic activity (a) without quenching agent, (b) isopropanol (c) silver nitrate (d) EDTA and (e) p-Benzoquinone (f) Quenching of active species on MG dye using SF-ZnS nanostructures.

3.13. Photodegradation of SSX and SMX using SF-ZnS nanostructures

The SF-ZnS nanostructures was investigated for the photodegradation of SSX and SMX pharmaceuticals as presented in figures 10(a)–(c). The absorption spectra for SSX and SMX irradiated in the presence of SF-ZnS nanostructures carried out at various time intervals showed a decrease in the intensity of the peak. This suggest that SSX and SMX have been decomposed by photocatalytic treatment. Upon testing the adsorption –desoption capabilities of the materials before the equilibrium was reached, a substantial amount of the SSX and SMX pollutants, respectively were adsorbed. Upon radiating the light on the solution, a maximum of 98% and 96% of SSX and SMX respectively was decayed in 120 min of reaction time. figure 10(d) suggests that the degradation of SMX followed the second order kinetics with the rate constant of 0.02922 min^{-1}. The R^2 value was found to be 0.9522 which is a better fit for second order kinetics.

Further, the plot of $In\left(\frac{Ao}{At}\right)$ was also used to get the rate constant of SF-ZnS nanostructures when decomposing SSX and it was found to be 0.0378 min^{-1} with an R^2 value of 0.87936. This R^2 results for SSX did not indicate correlation with Langmuir-Hinshelwood kinetic model. In comparison with other studies, Hu *et al* [36] found that TiO_2 was able to degrade 95% of the SMX. Similarly, in another study done by Abellan *et al* [37], the higher efficiency of SMX (82%) was also obtained when decomposing it using TiO_2. For the degradation of SSX, Hasan *at al* [38] reported that the photocatalytic test done using TiO_2 showed higher removal efficiency which was 93% over 1 h under irradiation. In their studies they reported that the OH which were produced on the aqueous-TiO_2 interface were the ones responsible for that higher degradation efficiency. Moreover, the tests were also done to support that the hydroxyl radicals were the active oxidizing agents for SMX. Though there are no studies where they have used SF-ZnS nanostructures for the decomposition of SSX and SMX from literature it was anticipated to get higher removal efficiency while using ZnS.

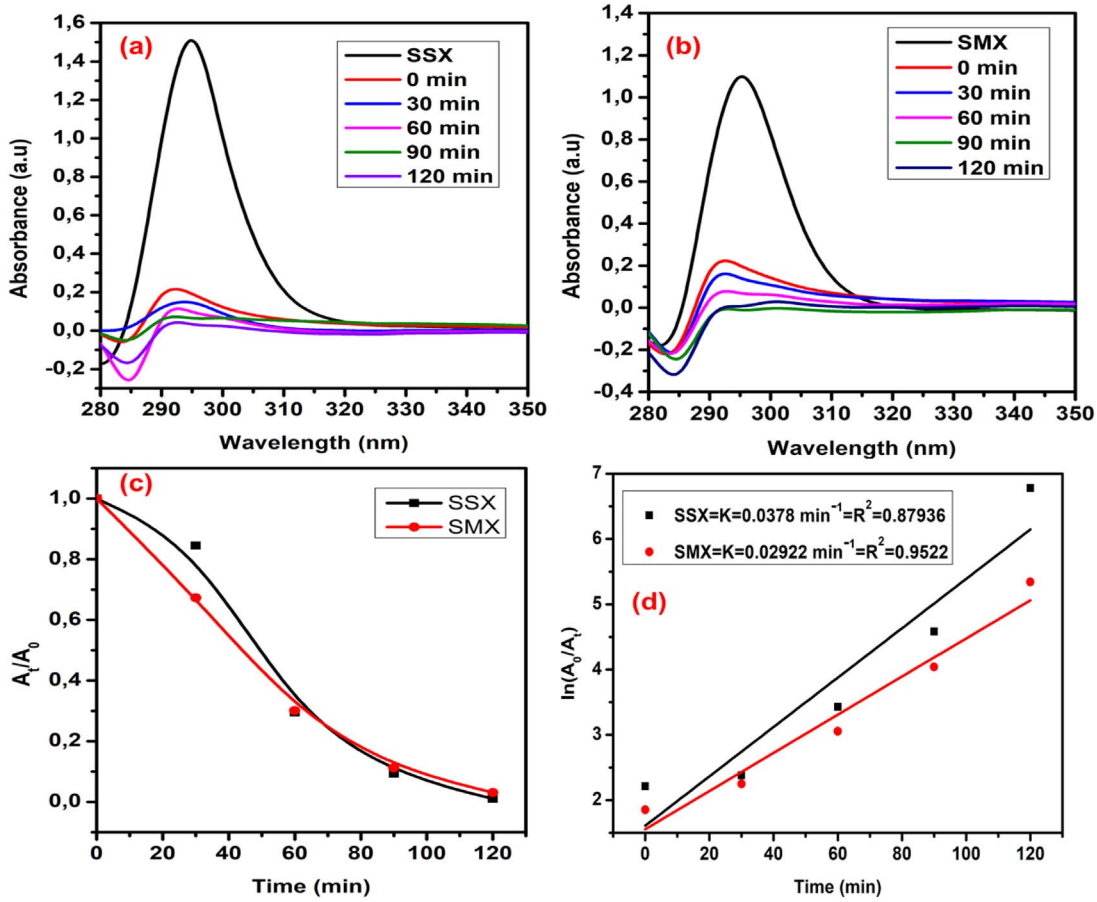

Figure 10. (a)–(c). The $\frac{A_t}{A_0}$ plot of SSX and SMX for SF-ZnS nanostructures (d) the kinetic studies for SSX and SMX.

4. Conclusion

The SF-ZnS nanostructures were synthesized by the green route using *S. fructescens* plant extract. X-ray diffraction pattern exhibited wurtzite hexagonal structure with an average size of 41.23 nm. The band gap energy estimated from the UV–vis absorption spectrum was found to be 3.6 eV. The FTIR results displayed the presence of O–H, C=O, C–O and C=N groups which acted as the stabilizing agent during the synthesis of SF-ZnS nanostructures. Thermal stability studies showed that the material was thermally stable up until 480 °C. The photocatalytic activity results showed that the SF-ZnS nanostructures were able to remove about 90% of the MG dye under irradiation. The holes were found to be the major species responsible for the degradation of MG using SF-ZnS nanostructures and they could be reused up to 3 times without losing much efficiency. Further, the SF-ZnS nanostructures evaluated for the SSX and SMX exhibited the maximum efficiency at 98% and 96% respectively. From these results, the SF-ZnS nanostructures showed to be a better photocatalyst which can be applied for the removal of different pollutants.

Acknowledgments

The authors would like to greatly acknowledge the DSI/NRF Centre of Excellence in Strong Materials under the Carbon nanotubes division for their continued financial support for student funding, analysis and running costs of the project. The department of chemistry at the University of Limpopo for lab space and instruments is also acknowledged. Lastly, this project would not have been possible without the funding of the Thuthuka NRF 117999.

Data availability statement

The data that support the findings of this study are available upon reasonable request from the authors.

Funding

This work was Funded by the DSI NRF Centre of Excellence in Strong Materials (Carbon nanotubes division) and THUTHUKA GRANT (UID: TTK-117999).

Conflicts of interest

The authors declare that there are no conflicts.

ORCID iDs

Lousia M Mahlaule Glory https://orcid.org/0000-0002-7746-0430
Nomso Charmaine Hintsho-Mbita https://orcid.org/0000-0002-0391-7573

References

[1] DeNicola E, Aburizaiza O S, Siddique A, Khwaja H and Carpenter D O 2015 Climate change and water scarcity: the case of Saudi Arabia *Annals of global health.* **81** 342–53
[2] Zhang S 2014 Preparation of controlled-shape ZnS microcrystals and photocatalytic property *Ceram. Int.* **40** 4553–7
[3] Makofane A, Motaung D E and Hintsho-Mbita N C 2021 Photocatalytic degradation of methylene blue and sulfisoxazole from water using biosynthesized zinc ferrite nanoparticles *Ceram. Int.* **47** 22615–26
[4] Bai H J, Zhang Z M and Gong J 2006 Biological synthesis of semiconductor zinc sulfide nanoparticles by immobilized Rhodobacter sphaeroides *Biotechnol. Lett* **28** 1135–9
[5] Salavati-Niasari M, Mohammad M, Loghman-Estarki R and Davar F 2009 Controllable synthesis of Wurtzite ZnS nanorods through simple hydrothermal method in the precense of thioglycolic acid *J. Alloys Compd.* **475** 782–8
[6] La Porta F *et al* 2013 Synthesis of wurtzite ZnS nanoparticles using the microwave assisted solvothermal method *J. Alloys Compd.* **556** 153–9
[7] Huo F, Wang Y, You C, Deng W, Yang F and Pu Y 2017 Phase-and size-controllable synthesis with efficient photocatalytic activity of ZnS nanoparticles *J. Mater. Sci.* **52** 5626–33
[8] Mahlaule-Glory L M, Mbita Z, Ntsendwana B, Mathipa M M, Mketo N and Hintsho-Mbita N C 2019 ZnO nanoparticles via *Sutherlandia frutescens* plant extract: physical and biological properties *Mater. Res. Express* **6** 085006
[9] Lei W, Browning J D Jr, Eichen P A, Brownstein K J, Folk W R, Sun G Y, Lubahn D B, Rottinghaus G E and Fritsche K L 2015 Unveiling the anti-inflammatory activity of *Sutherlandia frutescens* using murine macrophages *Int. Immunopharmacol.* **29** 254–62
[10] Kavitha K S, Baker S, Rakshith D, Kavitha H U, Yashwantha Rao H C, Harini B P and Satish S 2013 Plants as green source towards synthesis of nanoparticles *International Research Journal of Biological Sciences.* **2** 66–76
[11] Munyai S, Tetana Z N, Mathipa M M, Ntsendwana B and Hintsho-Mbita N C 2021 Green synthesis of Cadmium Sulphide nanoparticles for the photodegradation of Malachite green dye, Sulfisoxazole and removal of bacteria *Optik* **247** 167851
[12] Chen J, Hu B and Zhi J 2016 Optical and photocatalytic properties of Corymbia citriodora leaf extract synthesized ZnS nanoparticles *Physica E* **79** 103–6
[13] Senapati U S and Sarkar D 2015 Structural, spectral and electrical properties of green synthesized ZnS nanoparticles using elaeocarpus floribundus *J. Mater. Sci., Mater. Electron.* **26** 5783–91
[14] Ngoepe N M, Mathipa N M and Hintsho-Mbita N C 2020 Biosynthesis of titanium dioxide nanoparticles for the degradation of dyes and removal of bacteria *Optik* **224** 165728
[15] Sok J, Pineau N, Dalko-Csiba M, Breton L and Bernerd F 2008 Improvement of the dermal epidermal junction in human reconstructed skin by a new c-xylopyranoside derivative *European Journal of Dermatology.* **18** 297–302
[16] Kärkönen A, Dewhirst R A, Mackay C L and Fry S C 2017 Metabolites of 2, 3-diketogulonate delay peroxidase action and induce non-enzymic H_2O_2 generation: Potential roles in the plant cell wall *Arch. Biochem. Biophys.* **620** 12–22
[17] Miltojević A B, Stojanović N M, Randjelović P J and Radulović N S 2019 Distribution of methyl and isopropyl N-methylanthranilates and their metabolites in organs of rats treated with these two essential-oil constituents *Food Chem. Toxicol.* **128** 68–80
[18] Sathishkumar M, Saroja M, Venkatachalam M, Parthasarathy G and Rajamanickam A T 2017 Biosynthesis and characterization of zinc sulphide nanoparticles using leaf extracts of tridaxprocumbens *Orient. J. Chem.* **33** 903–9
[19] Kannan S, Subiramaniyam N P and Sathishkumar M 2020 Green synthesized zinc sulfide nanoparticles from Tridax procumbens plant extract for improved photocatalytic activity *Mater. Today Proc.* (https://doi.org/10.1016/j.matpr.2020.10.956)
[20] Khiew P S, Radiman S, Huang N M, Ahmad M S and Nadarajah K 2005 Preparation and characterization of ZnS nanoparticles synthesized from chitosan laurate micellar solution *Mater. Lett.* **59** 989–93
[21] Hussain I, Singh N B, Singh A, Singh H and Singh S C 2016 Green synthesis of nanoparticles and its potential application *Biotechnol. Lett* **38** 545–60
[22] Senapati U S and Sarkar D 2015 Synthesis and characterization of biopolymer protected zinc sulphide nanoparticles *Superlattices Microstruct.* **85** 722–33
[23] Senapati U S and Sarkar D 2014 Characterization of biosynthesized zinc sulphide nanoparticles using edible mushroom Pleurotuss ostreatu *Indian J. Phys.* **88** 557–62
[24] Caires A J, Mansur A A, Carvalho I C, Carvalho S M and Mansur H S 2020 Green synthesis of ZnS quantum dot/biopolymer photoluminescent nanoprobes for bioimaging brain cancer cells *Mater. Chem. Phys.* **244** 122716
[25] Munyai S and Hintsho-Mbita N C 2021 Green derived metal sulphides as photocatalysts for waste water treatment. A review *Current Research in Green and Sustainable Chemistry.* **4** 100163
[26] Samanta D, Basnet P, Chanu T I and Chatterjee S 2020 Biomolecule assisted morphology-controllable synthesis of Zinc Sulphide nanomaterials for efficient photocatalytic activity under solar irradiation *J. Alloys Compd.* **844** 155810

[27] Lalithadevi B, Rao K M and Ramananda D 2018 Investigations on structural and optical properties of starch capped ZnS nanoparticles synthesized by microwave irradiation method *Chem. Phys. Lett.* **700** 74–9
[28] Kannan S, Subiramaniyam N P and Sathishkumar M 2020 A novel green synthesis approach for improved photocatalytic activity and antibacterial properties of zinc sulfide nanoparticles using plant extract of Acalypha indica and Tridax procumbens *J. Mater. Sci., Mater. Electron.* **31** 9846–59
[29] Sharma S, Ameta R, Malkani R K and Ameta S C 2013 Photocatalytic degradation of rose Bengal by semiconducting zinc sulphide used as a photocatalyst *J. Serb. Chem. Soc.* **78** 897–905
[30] Raksha K R, Ananda S and Madegowda N M 2015 Study of kinetics of photocatalysis, bacterial inactivation and $^{\cdot}$OH scavenging activity of electrochemically synthesized Se4 + doped ZnS nanoparticles *J. Mol. Catal. A: Chem.* **396** 319–27
[31] Mani S K, Saroja M, Venkatachalam M and Rajamanickam T 2018 Antimicrobial activity and photocatalytic degradation properties of zinc sulfide nanoparticles synthesized by using plant extracts *Journal of Nanostructures.* **8** 107–18
[32] Samanta D, Chanu T I and Chatterjee S 2017 Citrus limetta juice as capping agent in hydrothermal synthesis of ZnS nanosphere for photocatalytic activity *Mater. Res. Bull.* **88** 85–90
[33] Kannan S, Subiramaniyam N P and Sathishkumar M 2020 Green synthesized zinc sulfide nanoparticles from Tridax procumbens plant extract for improved photocatalytic activity *Materials Today: Proceedings*
[34] Rajabi H R and Farsi M 2015 Effect of transition metal ion doping on the photocatalytic activity of ZnS quantum dots: synthesis, characterization, and application for dye decolorization *J. Mol. Catal. A: Chem.* **399** 53–61
[35] Wang H J, Cao Y, Wu L L, Wu S S, Raza A, Liu N, Wang J Y and Miyazawa T 2018 ZnS-based dual nano-semiconductors (ZnS/PbS, ZnS/CdS or ZnS/Ag2S,): a green synthesis route and photocatalytic comparison for removing organic dyes *J. Environ. Chem. Eng.* **6** 6771–9
[36] Hu L, Flanders P M, Miller P L and Strathmann T J 2007 Oxidation of sulfamethoxazole and related antimicrobial agents by TiO_2 photocatalysis *Water Res.* **41** 2612–26
[37] Abellán M N, Bayarri B, Giménez J and Costa J J A C B E 2007 Photocatalytic degradation of sulfamethoxazole in aqueous suspension of TiO2 *Appl. Catalysis B* **74** 233–41
[38] Hasan N, Moon G H, Park J, Park J and Kim J 2018 Visible light-induced degradation of sulfa drugs on pure TiO_2 through ligand-to-metal charge transfer *Sep. Purif. Technol.* **203** 242–50